Commun. Comput. Phys.
doi: 10.4208/cicp.120313.230813s

Vol. **15**, No. 4, pp. 959-980
April 2014

Finite Volume Hermite WENO Schemes for Solving the Hamilton-Jacobi Equation

Jun Zhu[1] and Jianxian Qiu[2,*]

[1] *College of Science, Nanjing University of Aeronautics and Astronautics, Nanjing 210016, Jiangsu, China.*
[2] *School of Mathematical Sciences, Xiamen University, Xiamen 361005, Fujian, China.*

Received 12 March 2013; Accepted (in revised version) 23 August 2013

Available online 21 January 2014

Abstract. In this paper, we present a new type of Hermite weighted essentially non-oscillatory (HWENO) schemes for solving the Hamilton-Jacobi equations on the finite volume framework. The cell averages of the function and its first one (in one dimension) or two (in two dimensions) derivative values are together evolved via time approaching and used in the reconstructions. And the major advantages of the new HWENO schemes are their compactness in the spacial field, purely on the finite volume framework and only one set of small stencils is used for different type of the polynomial reconstructions. Extensive numerical tests are performed to illustrate the capability of the methodologies.

AMS subject classifications: 65M06, 65M99, 35L65

Key words: HWENO scheme, finite volume, Hamilton-Jacobi equation.

1 Introduction

In this paper, we investigate using the finite volume Hermite weighted essentially non-oscillatory (HWENO) reconstruction methodologies for directly solving the Hamilton-Jacobi (H-J) equations:

$$\begin{cases} \phi_t + H(\nabla\phi) = 0, & (x_1,\cdots,x_n,t) \in \Omega\times[0,\infty), \\ \phi(x_1,\cdots,x_n,0) = \phi_0(x_1,\cdots,x_n), & (x_1,\cdots,x_n)\in\Omega, \end{cases} \tag{1.1}$$

where $\nabla\phi = (\phi_{x_1},\cdots,\phi_{x_n})^T$.

The Hamilton-Jacobi equations are often used in geometric optics, computer vision, material science, image processing and variational calculus [4, 13, 21]. Yet, the solutions to (1.1) are continuous but their derivatives are discontinuous. And such solutions may

*Corresponding author. *Email addresses:* `zhujun@nuaa.edu.cn` (J. Zhu), `jxqiu@xmu.edu.cn` (J. Qiu) not be unique unless using the physical implications and then getting the viscosity solutions [1]. It is well known that the HJ equations are closely related to conservation laws, hence we can obtain the exact solutions of HJ equations from those of conservation laws, respectively, and successful numerical methods for conservation laws can be adapted for solving the HJ equations. Along this line we mention the early works, Osher and Sethian [14] proposed a second order essentially non-oscillatory (ENO) scheme and Osher and Shu [15] presented high order ENO schemes to solve the Hamilton-Jacobi equations. Then, a high order of Weighted ENO (WENO) scheme was proposed by Jiang and Peng [7]. Recently, Qiu [16, 17] and with Shu [20] also proposed Hermite WENO schemes for solving the Hamilton-Jacobi equations on structured meshes. In 1996, Lafon and Osher [10] constructed the ENO schemes for solving the Hamilton-Jacobi equations on unstructured meshes. Zhang and Shu [25], Li and Chan [12] further developed high order WENO schemes for solving two dimensional Hamilton-Jacobi equations by using the nodal based weighted essentially non-oscillatory algebraic polynomial reconstructions on triangular meshes. And some finite element methods for arbitrary triangular meshes were developed in [2, 3, 6, 11]. Unlike the discontinuous Galerkin (DG) method of Hu and Shu [6] which applied DG framework on the conservation law system satisfied by the derivatives of the solution, Cheng and Shu presented DG methods to directly solve HJ equations (1.1) for ϕ in [5] and new flux was presented to keep stability of the method. In [24], a new DG method to directly solve HJ equations (1.1) was presented, in which local DG method was applied to approximate derivatives of ϕ.

This is a continuation paper for solving the Hamilton-Jacobi equations [7,16,17,20,25], following the (H)WENO methodologies for the conservation laws [18, 19, 26, 27]. We evolve both the cell averages of the viscosity solution ϕ and its derivatives over the target cell. Both the cell average of the solution and the cell averages of its derivatives are used to reconstruct the point values of the solution ϕ and its derivatives at different Gauss-Lobatto quadrature points on the target cell and its boundaries, respectively. Comparing with the original WENO schemes of Jiang and Peng [7], Qiu [16], Li and Chan [12], one major advantage of HWENO schemes [17, 20] is its compactness in the reconstructions, since both the solution and its derivatives are evolved in time. Also, the new HWENO schemes are more compact than the original HWENO schemes, e.g., [17, 20], easily in using the same one set of spacial stencils in the reconstructions and purely on the finite volume framework.

The organization of this paper is as follows: in Section 2, we review and construct the new finite volume HWENO schemes in 1D and 2D in detail for solving Hamilton-Jacobi equations and present extensive numerical results in Section 3 to verify the accuracy and stability of these approaches. Concluding remarks are given in Section 4.

2 The construction of HWENO schemes for the Hamilton-Jacobi equations

In this section, we give the framework for solving the Hamilton-Jacobi equations briefly and then develop the procedures of the HWENO schemes for both one and two dimensional Hamilton-Jacobi equations in detail.

2.1 The framework for one dimensional case

We take the control equations (1.1) in one dimension. For simplicity, we assume the computational field Ω has been divided as an uniform mesh with cells $I_i=[x_{i-1/2},x_{i+1/2}]$, $I_{i-1/2}=[x_{i-1},x_i]$, and $I_{i+1/2}=[x_i,x_{i+1}]$, $i=1,\cdots,N$. We denote $x_i=(x_{i-1/2}+x_{i+1/2})/2$ to be the cell center and $|I_i|=h$ to be the length of I_i, respectively. Let $u(x,t)=\phi_x(x,t)$. Taking the x derivative of (1.1), we can obtain the conservation laws:

$$\begin{cases} u_t+H(u)_x=0, \\ u(x,0)=\dfrac{d\phi_0(x)}{dx}. \end{cases} \tag{2.1}$$

We define the cell average $\bar{\phi}_i(t)=|I_i|^{-1}\int_{I_i}\phi(x,t)dx$ to be the numerical approximation to the viscosity solution of (1.1) over the target cell I_i and the cell average of u as $\bar{u}_i(t)=|I_i|^{-1}\int_{I_i}u(x,t)dx$. Integrate (1.1) and (2.1) over I_i, respectively, we obtain the equivalent formulations of the Hamilton-Jacobi equations:

$$\begin{cases} \dfrac{d}{dt}\bar{\phi}_i(t)=-\dfrac{1}{|I_i|}\displaystyle\int_{I_i}H(u(x,t))dx, \\ \dfrac{d}{dt}\bar{u}_i(t)=-\dfrac{1}{|I_i|}(H(u(x_{i+1/2},t))-H(u(x_{i-1/2},t))). \end{cases} \tag{2.2}$$

The integrals in (2.2) can be discretized by the following schemes:

$$\begin{cases} \dfrac{d}{dt}\bar{\phi}_i(t)=-\dfrac{1}{|I_i|}\hat{H}_i, \\ \dfrac{d}{dt}\bar{u}_i(t)=-\dfrac{1}{|I_i|}(\hat{H}_{i+1/2}-\hat{H}_{i-1/2}), \end{cases} \tag{2.3}$$

where $\hat{H}_i$ (see in [5]) is defined by:

$$\begin{aligned} \hat{H}_i=&\int_{I_i}H(u(x,t))dx+\frac{1}{2}\left(\min_{x\in I_{i+1/2}}H_1(u(x,t))-\left|\min_{x\in I_{i+1/2}}H_1(u(x,t))\right|\right)[\phi]_{i+1/2} \\ &+\frac{1}{2}\left(\max_{x\in I_{i-1/2}}H_1(u(x,t))+\left|\max_{x\in I_{i-1/2}}H_1(u(x,t))\right|\right)[\phi]_{i-1/2}, \end{aligned} \tag{2.4}$$

where we use the Gauss-Lobatto quadrature formula to calculate $\int_{I_i}H(u(x,t))dx$ numerically, denote $[\phi]_{i\pm1/2}=\phi(x^+_{i\pm1/2},t)-\phi(x^-_{i\pm1/2},t)$ to be the jump of $\phi(x,t)$ at the cell interfaces $x_{i\pm1/2}$ and $H_1=\partial H/\partial u$. And the simple Lax-Friedrichs flux is defined by:

$$\hat{H}_{i+1/2}=\frac{1}{2}\big(H(u^-_{i+1/2})+H(u^+_{i+1/2})-\alpha(u^+_{i+1/2}-u^-_{i+1/2})\big), \tag{2.5}$$

where $u^{\pm}_{i+1/2}$ are the numerical approximations to the point values of $u(x_{i+1/2},t)$ from the left and right, and $\alpha=\max_u|H'(u)|$, respectively.

We rewrite the ODEs (2.3) as the form:

$$U_t=L(U). \tag{2.6}$$

Then we use third order version TVD Runge-Kutta time discrete method [23]:

$$\begin{cases} U^{(1)}=U^n+\Delta t L(U^n), \\ U^{(2)}=\dfrac{3}{4}U^n+\dfrac{1}{4}U^{(1)}+\dfrac{1}{4}\Delta t L(U^{(1)}), \\ U^{n+1}=\dfrac{1}{3}U^n+\dfrac{2}{3}U^{(2)}+\dfrac{2}{3}\Delta t L(U^{(2)}), \end{cases} \tag{2.7}$$

to obtain fully discrete scheme both in space and time. And we would like to omit variable t in the following if not cause confusion.

The crucial procedures of the new HWENO scheme are proposed here, which use the cell values $\{\bar{\phi}_i\}$ and the cell averages $\{\bar{u}_i\}$ to obtain the point values $\{\phi^{\mp}_{i\pm1/2}\}$ and $\{u_{G_\ell}\}$. These reconstructions should be both high order accurate in smooth regions and essentially non-oscillatory adjacent to the discontinuities. We come up with the procedures of the reconstructions on the same set of small stencils in the following.

Reconstruction of $\{\phi^{\mp}_{i\pm1/2}\}$ by HWENO from $\{\bar{\phi}_i\}$ and $\{\bar{u}_i\}$

1. Given the small stencils $S_0=\{I_{i-1},I_i\}$, $S_1=\{I_i,I_{i+1}\}$, $S_2=\{I_{i-1},I_i,I_{i+1}\}$ and the bigger stencil $\mathcal{T}=\cup_{n=0}^2 S_n$, we construct Hermite cubic reconstruction polynomials $p_n(x)$, $n=0,1,2$ and a fifth-degree reconstruction polynomial $q(x)$ such that:

$$\frac{1}{|I_{i+n}|}\int_{I_{i+n}} p_0(x)dx=\bar{\phi}_{i+n}, \quad \frac{1}{|I_{i+n}|}\int_{I_{i+n}} p_0'(x)dx=\bar{u}_{i+n}, \quad n=-1,0, \tag{2.8a}$$

$$\frac{1}{|I_{i+n}|}\int_{I_{i+n}} p_1(x)dx=\bar{\phi}_{i+n}, \quad \frac{1}{|I_{i+n}|}\int_{I_{i+n}} p_1'(x)dx=\bar{u}_{i+n}, \quad n=0,1, \tag{2.8b}$$

$$\frac{1}{|I_{i+n}|}\int_{I_{i+n}} p_2(x)dx=\bar{\phi}_{i+n}, \quad n=-1,0,1, \quad \frac{1}{|I_i|}\int_{I_i} p_2'(x)dx=\bar{u}_i, \tag{2.8c}$$

and

$$\frac{1}{|I_{i+n}|}\int_{I_{i+n}} q(x)dx=\bar{\phi}_{i+n}, \quad \frac{1}{|I_{i+n}|}\int_{I_{i+n}} q'(x)dx=\bar{u}_{i+n}, \quad n=-1,0,1. \tag{2.9}$$

We only need the values of these polynomials at the points $x_{i\pm1/2}$, which have the following polynomial expressions:

$$\begin{aligned} p_0(x)=\big(&-(h^4(\bar{u}_{i-1}+2\bar{u}_i))+24(\bar{\phi}_{i-1}-\bar{\phi}_i)(x-x_i)^3-3h^3(\bar{\phi}_{i-1}-5\bar{\phi}_i+(\bar{u}_{i-1}\\ &-3\bar{u}_i)(x-x_i))+12h(x-x_i)^2(3\bar{\phi}_{i-1}-3\bar{\phi}_i+(\bar{u}_{i-1}+\bar{u}_i)(x-x_i))\\ &+6h^2(x-x_i)(-\bar{\phi}_{i-1}+\bar{\phi}_i+2(\bar{u}_{i-1}+2\bar{u}_i)(x-x_i))\big)/(12h^3), \end{aligned} \tag{2.10a}$$

$$
\begin{aligned}
p_1(x)=&\big(h^4(2\bar{u}_i+\bar{u}_{i+1})+24(\bar{\phi}_i-\bar{\phi}_{i+1})(x-x_i)^3+3h^3(5\bar{\phi}_i-\bar{\phi}_{i+1}+3\bar{u}_i(x-x_i)\\
&-\bar{u}_{i+1}(x-x_i))+12h(x-x_i)^2(-3\bar{\phi}_i+3\bar{\phi}_{i+1}+(\bar{u}_i+\bar{u}_{i+1})(x-x_i))\\
&-6h^2(x-x_i)(\bar{\phi}_i-\bar{\phi}_{i+1}+2(2\bar{u}_i+\bar{u}_{i+1})(x-x_i))\big)/(12h^3), \qquad (2.10b)\\
p_2(x)=&\big(3h^2(\bar{\phi}_{i-1}-\bar{\phi}_{i+1})(x-x_i)+12(-\bar{\phi}_{i-1}+\bar{\phi}_{i+1})(x-x_i)^3-h^3(\bar{\phi}_{i-1}-26\bar{\phi}_i\\
&+\bar{\phi}_{i+1}-30\bar{u}_i(x-x_i))+12h(x-x_i)^2(\bar{\phi}_{i-1}-2\bar{\phi}_i+\bar{\phi}_{i+1}\\
&-2\bar{u}_i(x-x_i))\big)/(24h^3). \qquad (2.10c)
\end{aligned}
$$

2. We compute the combination coefficients, the linear weights, denoted by $\gamma_n(x_{i\pm1/2})$, $n=0,1,2$, satisfying:

$$
q(x_{i\pm1/2})=\sum_{n=0}^{2}\gamma_n(x_{i\pm1/2})p_n(x_{i\pm1/2}), \qquad (2.11)
$$

for all possible cell average values $\bar{\phi}$ and cell averages $\bar{u}$ in the bigger stencil $\mathcal{T}$. These lead to:

$$
\begin{aligned}
&\gamma_0(x_{i+1/2})=\frac{3}{10}, \qquad \gamma_1(x_{i+1/2})=\frac{3}{10}, \qquad \gamma_2(x_{i+1/2})=\frac{4}{10}, \qquad (2.12a)\\
&\gamma_0(x_{i-1/2})=\frac{3}{10}, \qquad \gamma_1(x_{i-1/2})=\frac{3}{10}, \qquad \gamma_2(x_{i-1/2})=\frac{4}{10}. \qquad (2.12b)
\end{aligned}
$$

3. For the smaller stencils S_n, $n=0,1,2$, we compute the smoothness indicators, denoted by β_n, which measure how smooth the functions $p_n(x)$ are in the target cell I_i. The smaller these smoothness indicators, the smoother the functions are in the target cell I_i. We use the similar recipe for the smoothness indicators as in [8]:

$$
\beta_n=\sum_{\eta=1}^{3}\int_{I_i}|I_i|^{2\eta-1}\Big(\frac{d^\eta p_n(x)}{dx^\eta}\Big)^2dx, \quad n=0,1,2. \qquad (2.13)
$$

The formulas are explicitly expressed as:

$$
\begin{aligned}
\beta_0=&\big(11712\bar{\phi}_{i-1}^2+11712\bar{\phi}_i^2-12h\bar{\phi}_i(911\bar{u}_{i-1}+1041\bar{u}_i)-12\bar{\phi}_{i-1}(1952\bar{\phi}_i\\
&-911h\bar{u}_{i-1}-1041h\bar{u}_i)+h^2(2603\bar{u}_{i-1}^2+5726\bar{u}_{i-1}\bar{u}_i+3443\bar{u}_i^2)\big)/60, \qquad (2.14a)\\
\beta_1=&\big(11712\bar{\phi}_i^2+11712\bar{\phi}_{i+1}^2-12h\bar{\phi}_{i+1}(1041\bar{u}_i+911\bar{u}_{i+1})-12\bar{\phi}_i(1952\bar{\phi}_{i+1}\\
&-1041h\bar{u}_i-911h\bar{u}_{i+1})+h^2(3443\bar{u}_i^2+5726\bar{u}_i\bar{u}_{i+1}+2603\bar{u}_{i+1}^2)\big)/60, \qquad (2.14b)\\
\beta_2=&\big(2603\bar{\phi}_{i-1}^2+1040\bar{\phi}_i^2-1040\bar{\phi}_i\bar{\phi}_{i+1}+2603\bar{\phi}_{i+1}^2-9372h\bar{\phi}_{i+1}\bar{u}_i+9612h^2\bar{u}_i^2\\
&-2\bar{\phi}_{i-1}(520\bar{\phi}_i+2083\bar{\phi}_{i+1}-4686h\bar{u}_i)\big)/240. \qquad (2.14c)
\end{aligned}
$$

4. Then we compute the nonlinear weights based on the linear weights and smoothness indicators [22]:

$$
\omega_n(x_{i\pm1/2})=\frac{\overline{\omega}_n(x_{i\pm1/2})}{\sum_{k=0}^{2}\overline{\omega}_k(x_{i\pm1/2})}, \quad \overline{\omega}_n(x_{i\pm1/2})=\frac{\gamma_n(x_{i\pm1/2})}{\sum_{k=0}^{2}(\varepsilon+\beta_k)^2}, \quad n=0,1,2, \qquad (2.15)
$$

where $\gamma_n(x_{i\pm 1/2})$ are the linear weights determined in the above step, and ε is a small positive number to avoid division by 0. In this paper, we use $\varepsilon = 10^{-6}$ in all computations. The final approximations are given by:

$$\phi^{\mp}_{i\pm\frac{1}{2}} \approx \sum_{n=0}^{2} \omega_n(x_{i\pm\frac{1}{2}}) p_n(x_{i\pm\frac{1}{2}}). \tag{2.16}$$

Reconstruction of $\{u_{G_\ell}\}$ by HWENO from $\{\bar{\phi}_i\}$ and $\{\bar{u}_i\}$

1. Given the same stencils $S_0=\{I_{i-1},I_i\}$, $S_1=\{I_i,I_{i+1}\}$, $S_2=\{I_{i-1},I_i,I_{i+1}\}$ and the bigger stencil $\aleph=\cup_{n=0}^{2} S_n$, we construct the same Hermite cubic reconstruction polynomials $p_n(x)$, $n=0,1,2$ and the same fifth-degree reconstruction polynomial $q(x)$ satisfying (2.8a), (2.8b), (2.8c) and (2.9). In this paper, we only need the values of the derivative of these polynomials at different four Gauss-Lobatto quadrature points x_{G_ℓ} such as $x_{i-1/2}$, $x_{i-\sqrt{5}/10}$, $x_{i+\sqrt{5}/10}$ and $x_{i+1/2}$, which have the following polynomial expressions:

$$\begin{aligned} p_0'(x) = \big(&-(h^3(\bar{u}_{i-1}-3\bar{u}_i)) + 24(\bar{\phi}_{i-1}-\bar{\phi}_i)(x-x_i)^2 + 12h(x-x_i)(2\bar{\phi}_{i-1}-2\bar{\phi}_i(x-x_i)) \\ &+ (\bar{u}_{i-1}+\bar{u}_i) + 2h^2(-\bar{\phi}_{i-1}+\bar{\phi}_i+4(\bar{u}_{i-1}+2\bar{u}_i)(x-x_i)))\big)/(4h^3), \end{aligned} \tag{2.17a}$$

$$\begin{aligned} p_1'(x) = \big(&h^3(3\bar{u}_i-\bar{u}_{i+1}) + 24(\bar{\phi}_i-\bar{\phi}_{i+1})(x-x_i)^2 + 12h(x-x_i)(-2\bar{\phi}_i+2\bar{\phi}_{i+1} \\ &-2h^2(\bar{\phi}_i-\bar{\phi}_{i+1}+4(2\bar{u}_i+\bar{u}_{i+1})(x-x_i))))\big)/(4h^3), \end{aligned} \tag{2.17b}$$

$$\begin{aligned} p_2'(x) = \big(&h^2(\bar{\phi}_{i-1}-\bar{\phi}_{i+1}) + 10h^3\bar{u}_i + 12(-\bar{\phi}_{i-1}+\bar{\phi}_{i+1})(x-x_i)^2 \\ &+8h(x-x_i)(\bar{\phi}_{i-1}-2\bar{\phi}_i+\bar{\phi}_{i+1}-3\bar{u}_i(x-x_i))\big)/(8h^3). \end{aligned} \tag{2.17c}$$

2. We compute the linear weights by requiring:

$$q'(x_{G_\ell}) = \sum_{n=0}^{2} \gamma_n^x(x_{G_\ell}) p_n'(x_{G_\ell}), \quad \ell=1,2,3,4, \tag{2.18}$$

for all possible cell average values $\bar{\phi}$ and cell averages $\bar{u}$ in the bigger stencil $\aleph$. These lead to:

$$\gamma_0^x(x_{G_1}) = \frac{5}{6}, \qquad \gamma_1^x(x_{G_1}) = \frac{1}{18}, \qquad \gamma_2^x(x_{G_1}) = \frac{1}{9}, \tag{2.19a}$$

$$\gamma_0^x(x_{G_2}) = \frac{220-41\sqrt{5}}{570}, \qquad \gamma_1^x(x_{G_2}) = \frac{220+41\sqrt{5}}{570}, \qquad \gamma_2^x(x_{G_2}) = \frac{13}{57}, \tag{2.19b}$$

$$\gamma_0^x(x_{G_3}) = \frac{220+41\sqrt{5}}{570}, \qquad \gamma_1^x(x_{G_3}) = \frac{220-41\sqrt{5}}{570}, \qquad \gamma_2^x(x_{G_3}) = \frac{13}{57}, \tag{2.19c}$$

$$\gamma_0^x(x_{G_4}) = \frac{1}{18}, \qquad \gamma_1^x(x_{G_4}) = \frac{5}{6}, \qquad \gamma_2^x(x_{G_4}) = \frac{1}{9}. \tag{2.19d}$$

3. We compute the smoothness indicators [20, 25]:

$$\beta_n^x = \sum_{\eta=1}^{3} \int_{I_i} |I_i|^{2\eta-1} \Big(\frac{d^\eta}{dx^\eta} \frac{dp_n(x)}{dx} \Big)^2 dx, \quad n=0,1,2, \tag{2.20}$$

obtaining:

$$\beta_0^x = \big(192\bar{\phi}_{i-1}^2 + 192\bar{\phi}_i^2 - 12h\bar{\phi}_i(15\bar{u}_{i-1} + 17\bar{u}_i) + 12\bar{\phi}_{i-1}(-32\bar{\phi}_i + 15h\bar{u}_{i-1} + 17h\bar{u}_i) + h^2(43\bar{u}_{i-1}^2 + 94\bar{u}_{i-1}\bar{u}_i + 55\bar{u}_i^2)\big)/h^2, \tag{2.21a}$$

$$\beta_1^x = \big(192\bar{\phi}_i^2 + 192\bar{\phi}_{i+1}^2 - 12h\bar{\phi}_{i+1}(17\bar{u}_i + 15\bar{u}_{i+1}) + 12\bar{\phi}_i(-32\bar{\phi}_{i+1} + 17h\bar{u}_i + 15h\bar{u}_{i+1}) + h^2(55\bar{u}_i^2 + 94\bar{u}_i\bar{u}_{i+1} + 43\bar{u}_{i+1}^2)\big)/h^2, \tag{2.21b}$$

$$\beta_2^x = \big(43\bar{\phi}_{i-1}^2/4 + 4\bar{\phi}_i^2 - 4\bar{\phi}_i\bar{\phi}_{i+1} + 43\bar{\phi}_{i+1}^2/4 - 39h\bar{\phi}_{i+1}\bar{u}_i + 39h^2\bar{u}_i^2 + \bar{\phi}_{i-1}(-4\bar{\phi}_i - 35\bar{\phi}_{i+1}/2 + 39h\bar{u}_i)\big)/h^2. \tag{2.21c}$$

4. We compute the nonlinear weights by (2.15). The final HWENO reconstructions to u_{G_ℓ} are then given by:

$$u_{G_\ell} \approx \sum_{n=0}^{2} \omega_n^x(x_{G_\ell}) \frac{d}{dx} p_n(x_{G_\ell}), \quad \ell = 1,2,3,4. \tag{2.22}$$

2.2 The framework for two dimensional case

We take the control equations (1.1) in two dimensions. For simplicity, we also assume Ω has been divided as an uniform mesh with cells $I_{ij} = [x_{i-1/2}, x_{i+1/2}] \times [y_{j-1/2}, y_{j+1/2}]$, $J_i = [x_{i-1/2}, x_{i+1/2}]$, $K_j = [y_{j-1/2}, y_{j+1/2}]$, $J_{i+1/2} = [x_i, x_{i+1}]$ and $K_{j+1/2} = [y_j, y_{j+1}]$, $i = 1, \cdots, N$, $j = 1, \cdots, M$. We denote $(x_i, y_j) = ((x_{i-1/2} + x_{i+1/2})/2, (y_{j-1/2} + y_{j+1/2})/2)$, $|I_{ij}| = (x_{i+1/2} - x_{i-1/2})(y_{j+1/2} - y_{j-1/2}) = h^2$, $|J_i| = x_{i+1/2} - x_{i-1/2} = h$ and $|K_j| = y_{j+1/2} - y_{j-1/2} = h$ to be the cell center, the area of I_{ij}, the length of J_i and the length of K_j, respectively. Let $u(x,y,t) = \phi_x(x,y,t)$ and $v(x,y,t) = \phi_y(x,y,t)$. Taking the x, y derivatives of (1.1), we can obtain the conservation laws:

$$\begin{cases} u_t + H(u,v)_x = 0, \\ u(x,y,0) = \dfrac{\partial \phi_0(x,y)}{\partial x}, \end{cases} \tag{2.23}$$

and

$$\begin{cases} v_t + H(u,v)_y = 0, \\ v(x,y,0) = \dfrac{\partial \phi_0(x,y)}{\partial y}. \end{cases} \tag{2.24}$$

We define $\bar{\phi}_{ij}(t) = |I_{ij}|^{-1} \int_{I_{ij}} \phi(x,y,t) dxdy$ to be the numerical approximation to the viscosity solution of (1.1) of the target cell I_{ij}, the cell average of u as $\bar{u}_{ij}(t) = |I_{ij}|^{-1} \int_{I_{ij}} u(x,y,t) dxdy$ and the cell average of v as $\bar{v}_{ij}(t) = |I_{ij}|^{-1} \int_{I_{ij}} v(x,y,t) dxdy$. Integrate (1.1), (2.23) and (2.24) over the target cell I_{ij}, respectively, we obtain the equivalent formulations of the

Hamilton-Jacobi equations:

$$\begin{cases} \dfrac{d}{dt}\bar{\phi}_{ij}(t) = -\dfrac{1}{|I_{ij}|}\displaystyle\int_{I_{ij}} H(u(x,y,t),v(x,y,t))dxdy, \\ \dfrac{d}{dt}\bar{u}_{ij}(t) = -\dfrac{1}{|I_{ij}|}\Big(\displaystyle\int_{K_j} H(u(x_{i+1/2},y,t),v(x_{i+1/2},y,t))dy \\ \qquad\qquad -\displaystyle\int_{K_j} H(u(x_{i-1/2},y,t),v(x_{i-1/2},y,t))dy\Big), \\ \dfrac{d}{dt}\bar{v}_{ij}(t) = -\dfrac{1}{|I_{ij}|}\Big(\displaystyle\int_{J_i} H(u(x,y_{j+1/2},t),v(x,y_{j+1/2},t))dx \\ \qquad\qquad -\displaystyle\int_{J_i} H(u(x,y_{j-1/2},t),v(x,y_{j-1/2},t))dx\Big). \end{cases} \tag{2.25}$$

The latter two integrals in (2.25) can be discretized by a four-point Gauss-Lobatto integration formula on every edge and we approximate (2.25) by the following schemes:

$$\begin{cases} \dfrac{d}{dt}\bar{\phi}_{ij}(t) = -\dfrac{1}{|I_{ij}|}\hat{H}_{ij}, \\ \dfrac{d}{dt}\bar{u}_{ij}(t) = -\dfrac{|K_j|}{|I_{ij}|}\displaystyle\sum_{\ell=1}^{4}\sigma_\ell(\hat{H}(u(x_{i+1/2},y_{G_\ell},t),v(x_{i+1/2},y_{G_\ell},t)) \\ \qquad\qquad -\hat{H}(u(x_{i-1/2},y_{G_\ell},t),v(x_{i-1/2},y_{G_\ell},t))), \\ \frac{d}{dt}\bar{v}_{ij}(t) = -\dfrac{|J_i|}{|I_{ij}|}\displaystyle\sum_{\ell=1}^{4}\sigma_\ell(\hat{H}(u(x_{G_\ell},y_{j+1/2},t),v(x_{G_\ell},y_{j+1/2},t)) \\ \qquad\qquad -\hat{H}(u(x_{G_\ell},y_{j-1/2},t),v(x_{G_\ell},y_{j-1/2},t))), \end{cases} \tag{2.26}$$

where σ_l are the quadrature coefficients and $\hat{H}_{ij}$ is a global numerical Hamiltonian [5] and defined as:

$$\begin{aligned} \hat{H}_{ij} = & \int_{I_{ij}} H(u(x,y,t),v(x,y,t))dxdy + \frac{1}{2}\int_{K_j}\Big(\min_{x\in J_{i+1/2}} H_1(u(x,y,t),\overline{v(x,y,t)}) \\ & -\Big|\min_{x\in J_{i+1/2}} H_1(u(x,y,t),\overline{v(x,y,t)})\Big|\Big)[\phi](x_{i+1/2},y)dy \\ & +\frac{1}{2}\int_{K_j}\Big(\max_{x\in J_{i-1/2}} H_1(u(x,y,t),\overline{v(x,y,t)}) \\ & +\Big|\max_{x\in J_{i-1/2}} H_1(u(x,y,t),\overline{v(x,y,t)})\Big|\Big)[\phi](x_{i-1/2},y)dy \\ & +\frac{1}{2}\int_{J_i}\Big(\min_{y\in K_{j+1/2}} H_2(\overline{u(x,y,t)},v(x,y,t)) \\ & -\Big|\min_{y\in K_{j+1/2}} H_2(\overline{u(x,y,t)},v(x,y,t))\Big|\Big)[\phi](x,y_{j+1/2})dx \end{aligned}$$

$$+\frac{1}{2}\int_{J_i}\Big(\max_{y\in K_{j-1/2}} H_2(\overline{u(x,y,t)},v(x,y,t))$$
$$+\Big|\max_{y\in K_{j-1/2}} H_2(\overline{u(x,y,t)},v(x,y,t))\Big|\Big)[\phi](x,y_{j-1/2})dx, \tag{2.27}$$

where $\int_{I_{ij}} H(u(x,y,t),v(x,y,t))dxdy$ is calculated numerically by using a two dimensional Gauss-Lobatto quadrature formula, $\overline{u(x,y,t)}=(u^+(x,y,t)+u^-(x,y,t))/2$, $\overline{v(x,y,t)}=(v^+(x,y,t)+v^-(x,y,t))/2$, $[\phi](x_{i\pm1/2},y)=\phi(x^+_{i\pm1/2},y,t)-\phi(x^-_{i\pm1/2},y,t)$ and $[\phi](x,y_{j\pm1/2})=\phi(x,y^+_{j\pm1/2},t)-\phi(x,y^-_{j\pm1/2},t)$. And H_1 and H_2 are the partial derivatives of H with respect to ϕ_x and ϕ_y, otherwise are the Lipschitz constants of H globally (if not differentiable). We set $\alpha=\max\{\alpha_x,\alpha_y\}=\max\{\max|H_1|,\max|H_2|\}$. $\hat{H}(u(x_{i\pm1/2},y_{G_\ell},t),\, v(x_{i\pm1/2},y_{G_\ell},t))$ and $\hat{H}(u(x_{G_\ell},y_{j\pm1/2},t),\, v(x_{G_\ell},y_{j\pm1/2},t))$ are replaced by the numerical fluxes such as the Lax-Friedrichs fluxes:

$$\begin{aligned}&\hat{H}(u(x_{i\pm1/2},y_{G_\ell},t),v(x_{i\pm1/2},y_{G_\ell},t))\\ =&\frac{1}{2}\big\{H(u^-(x_{i\pm1/2},y_{G_\ell},t),v^-(x_{i\pm1/2},y_{G_\ell},t))+H(u^+(x_{i\pm1/2},y_{G_\ell},t),v^+(x_{i\pm1/2},y_{G_\ell},t))\\ &-\alpha_x(u^+(x_{i\pm1/2},y_{G_\ell},t)-u^-(x_{i\pm1/2},y_{G_\ell},t))\big\},\quad \ell=1,2,3,4,\end{aligned} \tag{2.28}$$

and

$$\begin{aligned}&\hat{H}(u(x_{G_\ell},y_{j\pm1/2},t),v(x_{G_\ell},y_{j\pm1/2},t))\\ =&\frac{1}{2}\big\{H(u^-(x_{G_\ell},y_{j\pm1/2},t),v^-(x_{G_\ell},y_{j\pm1/2},t))+H(u^+(x_{G_\ell},y_{j\pm1/2},t),v^+(x_{G_\ell},y_{j\pm1/2},t))\\ &-\alpha_y(v^+(x_{G_\ell},y_{j\pm1/2},t)-v^-(x_{G_\ell},y_{j\pm1/2},t))\big\},\quad \ell=1,2,3,4.\end{aligned} \tag{2.29}$$

We rewrite the ODEs (2.26) as the form of (2.6).

Then we use third order version TVD Runge-Kutta time discrete method (2.7) to obtain fully discrete scheme both in space and time.

Also, we use the cell values $\{\bar{\phi}_{ij}\}$, $\{\bar{u}_{ij}\}$ and $\{\bar{v}_{ij}\}$ to reconstruct the point values of $\{\phi(x^\mp_{i\pm1/2},y_{G_\ell},t)\}$, $\{\phi(x_{G_\ell},y^\mp_{j\pm1/2},t)\}$, $\{u(x_{G_\ell},y_{G_{\ell\ell}},t)\}$ and $\{v(x_{G_\ell},y_{G_{\ell\ell}},t)\}$, respectively. These reconstructions should be both high order accurate in smooth regions and essentially non-oscillatory adjacent to the discontinuities. We would like to omit variable t in the following if not cause confusion.

Reconstruction of $\{\phi^\mp_{i\pm1/2,G_\ell}\}$ and $\{\phi^\mp_{G_\ell,j\pm1/2}\}$ by HWENO from $\{\bar{\phi}_{ij}\}$, $\{\bar{u}_{ij}\}$ and $\{\bar{v}_{ij}\}$

1. We construct Hermite cubic reconstruction polynomials $p_n(x,y)$, $n=1,\cdots,12$, such that:

$$\frac{1}{|I_{k_1,k_2}|}\int_{I_{k_1,k_2}} p_n(x,y)dxdy=\bar{\phi}_{k_1,k_2}, \qquad n=1,\cdots,12, \tag{2.30a}$$
$$\frac{1}{|I_{k_3,k_4}|}\int_{I_{k_3,k_4}} \frac{\partial}{\partial x}p_n(x,y)dxdy=\bar{u}_{k_3,k_4}, \qquad n=1,\cdots,12, \tag{2.30b}$$

$$\frac{1}{|I_{k_5,k_6}|}\int_{I_{k_5,k_6}}\frac{\partial}{\partial y}p_n(x,y)dxdy=\bar{v}_{k_5,k_6}, \qquad n=1,\cdots,12, \tag{2.30c}$$

where

$$n=1, \qquad \begin{cases} (k_1,k_2)=(i-1,j-1),(i,j-1),(i-1,j),(i,j), \\ (k_3,k_4)=(i-1,j-1),(i-1,j),(i,j), \\ (k_5,k_6)=(i-1,j-1),(i,j-1),(i,j); \end{cases}$$

$$n=2, \qquad \begin{cases} (k_1,k_2)=(i,j-1),(i+1,j-1),(i,j),(i+1,j), \\ (k_3,k_4)=(i+1,j-1),(i,j),(i+1,j), \\ (k_5,k_6)=(i,j-1),(i+1,j-1),(i,j); \end{cases}$$

$$n=3, \qquad \begin{cases} (k_1,k_2)=(i-1,j),(i,j),(i-1,j+1),(i,j+1), \\ (k_3,k_4)=(i-1,j),(i,j),(i-1,j+1), \\ (k_5,k_6)=(i,j),(i-1,j+1),(i,j+1); \end{cases}$$

$$n=4, \qquad \begin{cases} (k_1,k_2)=(i,j),(i+1,j),(i,j+1),(i+1,j+1), \\ (k_3,k_4)=(i,j),(i+1,j),(i+1,j+1), \\ (k_5,k_6)=(i,j),(i,j+1),(i+1,j+1); \end{cases}$$

$$n=5, \qquad \begin{cases} (k_1,k_2)=(i-1,j-1),(i,j-1),(i+1,j-1),(i-1,j),(i,j),(i-1,j+1), \\ (k_3,k_4)=(i-1,j),(i,j), \\ (k_5,k_6)=(i,j-1),(i,j); \end{cases}$$

$$n=6, \qquad \begin{cases} (k_1,k_2)=(i-1,j-1),(i,j-1),(i+1,j-1),(i,j),(i+1,j),(i+1,j+1), \\ (k_3,k_4)=(i,j),(i+1,j), \\ (k_5,k_6)=(i,j-1),(i,j); \end{cases}$$

$$n=7, \qquad \begin{cases} (k_1,k_2)=(i-1,j-1),(i-1,j),(i,j),(i-1,j+1),(i,j+1),(i+1,j+1), \\ (k_3,k_4)=(i-1,j),(i,j), \\ (k_5,k_6)=(i,j),(i,j+1); \end{cases}$$

$$n=8, \qquad \begin{cases} (k_1,k_2)=(i+1,j-1),(i,j),(i+1,j),(i-1,j+1),(i,j+1),(i+1,j+1), \\ (k_3,k_4)=(i,j),(i+1,j), \\ (k_5,k_6)=(i,j),(i,j+1); \end{cases}$$

$$n=9, \qquad \begin{cases} (k_1,k_2)=(i-1,j-1),(i,j-1),(i+1,j-1),(i-1,j),(i,j),(i-1,j+1), \\ (k_3,k_4)=(i-1,j-1),(i,j), \\ (k_5,k_6)=(i-1,j-1),(i,j); \end{cases}$$

$$n=10, \qquad \begin{cases} (k_1,k_2)=(i-1,j-1),(i,j-1),(i+1,j-1),(i,j),(i+1,j),(i+1,j+1), \\ (k_3,k_4)=(i,j),(i+1,j-1), \\ (k_5,k_6)=(i+1,j-1),(i,j); \end{cases}$$

$$n=11, \qquad \begin{cases} (k_1,k_2)=(i-1,j-1),(i-1,j),(i,j),(i-1,j+1),(i,j+1),(i+1,j+1), \\ (k_3,k_4)=(i-1,j+1),(i,j), \\ (k_5,k_6)=(i,j),(i-1,j+1); \end{cases}$$

$$n=12,\qquad \begin{cases} (k_1,k_2)=(i+1,j-1),(i,j),(i+1,j),(i-1,j+1),(i,j+1),(i+1,j+1),\\ (k_3,k_4)=(i,j),(i+1,j+1),\\ (k_5,k_6)=(i,j),(i+1,j+1). \end{cases}$$

2. We compute the cubic polynomials to obtain a fifth-order approximation of $\phi(x,y)$ at the interfacial Gauss-Lobatto quadrature points $(x^{\mp}_{i\pm1/2},y_{G_\ell})$ and $(x_{G_\ell},y^{\mp}_{j\pm1/2})$, respectively. If we choose the combination coefficients, the linear weights, denoted by $\gamma_n(x_{i\pm1/2},y_{G_\ell})$ and $\gamma_n(x_{G_\ell},y_{j\pm1/2})$, $n=1,\cdots,12$, satisfying:

$$\phi(x^{\mp}_{i\pm1/2},y_{G_\ell})=\sum_{n=1}^{12}\gamma_n(x_{i\pm1/2},y_{G_\ell})p_n(x_{i\pm1/2},y_{G_\ell}),\quad \ell=1,2,3,4, \tag{2.31}$$

and

$$\phi(x_{G_\ell},y^{\mp}_{j\pm1/2})=\sum_{n=1}^{12}\gamma_n(x_{G_\ell},y_{j\pm1/2})p_n(x_{G_\ell},y_{j\pm1/2}),\quad \ell=1,2,3,4, \tag{2.32}$$

are valid for any polynomial ϕ of degree at most five, then we can obtain a fifth-order approximation of ϕ at different points for all sufficiently smooth functions. Notice that (2.31) and (2.32) hold for any polynomial ϕ of degree at most three if $\sum_{n=1}^{12}\gamma_n(x_{i\pm1/2},y_{G_\ell})=1$ and $\sum_{n=1}^{12}\gamma_n(x_{G_\ell},y_{j\pm1/2})=1$, $\ell=1,2,3,4$, respectively. This is because each individual $p_n(x,y)$ reconstructs cubic polynomials exactly. There are eleven other constraints on the linear weights from requiring (2.31) and (2.32) to hold for $\phi=(\frac{x-x_i}{|J_i|})^5$, $(\frac{x-x_i}{|J_i|})^4(\frac{y-y_j}{|K_j|})$, $(\frac{x-x_i}{|J_i|})^3(\frac{y-y_j}{|K_j|})^2$, $(\frac{x-x_i}{|J_i|})^2(\frac{y-y_j}{|K_j|})^3$, $(\frac{x-x_i}{|J_i|})(\frac{y-y_j}{|K_j|})^4$, $(\frac{y-y_j}{|K_j|})^5$, $(\frac{x-x_i}{|J_i|})^4$, $(\frac{x-x_i}{|J_i|})^3(\frac{y-y_j}{|K_j|})$, $(\frac{x-x_i}{|J_i|})^2(\frac{y-y_j}{|K_j|})^2$, $(\frac{x-x_i}{|J_i|})(\frac{y-y_j}{|K_j|})^3$ and $(\frac{y-y_j}{|K_j|})^4$. Fortunately, these twelve parameters can be determined by the twelve constraints mentioned above.

3. We compute the smoothness indicators, denoted by β_n, which measure how smooth the functions $p_n(x)$ are in the target cell I_{ij}. The smaller these smoothness indicators, the smoother the functions are in the target cell I_{ij}. We use the similar recipe for the smoothness indicators as in [8]:

$$\beta_n=\sum_{|\eta|=1}^{3}\int_{I_{ij}}|I_{ij}|^{|\eta|-1}\Big(\frac{\partial^{|\eta|}}{\partial x^{\eta_1}\partial y^{\eta_2}}p_n(x,y)\Big)^2dxdy,\quad n=1,\cdots,12. \tag{2.33}$$

4. Then we compute the nonlinear weights (2.15) based on the linear weights and smoothness indicators [22]. The final approximations are given by:

$$\phi^{\mp}_{i\pm\frac12,G_\ell}\approx\sum_{n=1}^{12}\omega_n(x_{i\pm\frac12},y_{G_\ell})p_n(x_{i\pm\frac12},y_{G_\ell}),\quad \ell=1,2,3,4, \tag{2.34}$$

and

$$\phi^{\mp}_{G_\ell,j\pm\frac12}\approx\sum_{n=1}^{12}\omega_n(x_{G_\ell},y_{j\pm\frac12})p_n(x_{G_\ell},y_{j\pm\frac12}),\quad \ell=1,2,3,4. \tag{2.35}$$

Reconstruction of $\{u_{G_\ell,G_{\ell\ell}}\}$ and $\{v_{G_\ell,G_{\ell\ell}}\}$ by HWENO from $\{\bar{\phi}_{ij}\}$, $\{\bar{u}_{ij}\}$ and $\{\bar{v}_{ij}\}$

1. Given the same polynomials $p_n(x,y)$, $n=1,\cdots,12$. In this paper, we only need the values of the derivative of these polynomials at different sixteen Gauss-Lobatto quadrature points $(x_{G_\ell},y_{G_{\ell\ell}})$, $\ell=1,2,3,4$, $\ell\ell=1,2,3,4$, which are the tensor product of one dimensional Gauss-Lobatto quadrature points.

2. We compute the linear weights by requiring:

$$u(x_{G_\ell},y_{G_{\ell\ell}})=\sum_{n=1}^{12}\gamma_n^x(x_{G_\ell},y_{G_{\ell\ell}})\frac{\partial}{\partial x}p_n(x_{G_\ell},y_{G_{\ell\ell}}),\quad \ell,\ell\ell=1,2,3,4, \tag{2.36}$$

and

$$v(x_{G_\ell},y_{G_{\ell\ell}})=\sum_{n=1}^{12}\gamma_n^y(x_{G_\ell},y_{G_{\ell\ell}})\frac{\partial}{\partial y}p_n(x_{G_\ell},y_{G_{\ell\ell}}),\quad \ell,\ell\ell=1,2,3,4, \tag{2.37}$$

are valid for any polynomial ϕ of degree at most five, then we can obtain fifth-order approximations of $u(x,y)$ and $v(x,y)$ at different points for all sufficiently smooth functions. Notice that (2.36) and (2.37) hold for any polynomial ϕ of degree at most three if $\sum_{n=1}^{12}\gamma_n^x(x_{G_\ell},y_{G_{\ell\ell}})=1$ and $\sum_{n=1}^{12}\gamma_n^y(x_{G_\ell},y_{G_{\ell\ell}})=1$, ℓ, $\ell\ell=1,2,3,4$, respectively. This is because each individual $p_n(x,y)$ reconstructs cubic polynomials exactly. There are eleven other constraints on the linear weights from requiring (2.36) and (2.37) to hold for $\phi=(\frac{x-x_i}{|J_i|})^5$, $(\frac{x-x_i}{|J_i|})^4(\frac{y-y_j}{|K_j|})$, $(\frac{x-x_i}{|J_i|})^3(\frac{y-y_j}{|K_j|})^2$, $(\frac{x-x_i}{|J_i|})^2(\frac{y-y_j}{|K_j|})^3$, $(\frac{x-x_i}{|J_i|})(\frac{y-y_j}{|K_j|})^4$, $(\frac{y-y_j}{|K_j|})^5$, $(\frac{x-x_i}{|J_i|})^4$, $(\frac{x-x_i}{|J_i|})^3(\frac{y-y_j}{|K_j|})$, $(\frac{x-x_i}{|J_i|})^2(\frac{y-y_j}{|K_j|})^2$, $(\frac{x-x_i}{|J_i|})(\frac{y-y_j}{|K_j|})^3$ and $(\frac{y-y_j}{|K_j|})^4$. Fortunately, these twelve parameters can be determined by the twelve constraints mentioned above.

3. We compute the smoothness indicators, denoted by β_n^x and β_n^y, which measure how smooth the functions $\partial p_n(x)/\partial x$ and $\partial p_n(x)/\partial y$ are in the target cell I_{ij}. The smaller these smoothness indicators, the smoother the functions are in the target cell I_{ij}. We use the similar recipe for the smoothness indicators as in [20,25]:

$$\beta_n^x=\sum_{|\eta|=1}^{3}\int_{I_{ij}}|I_{ij}|^{|\eta|-1}\Big(\frac{\partial^{|\eta|}}{\partial x^{\eta_1}\partial y^{\eta_2}}\frac{\partial}{\partial x}p_n(x,y)\Big)^2dxdy,\quad n=1,\cdots,12, \tag{2.38}$$

and

$$\beta_n^y=\sum_{|\eta|=1}^{3}\int_{I_{ij}}|I_{ij}|^{|\eta|-1}\Big(\frac{\partial^{|\eta|}}{\partial x^{\eta_1}\partial y^{\eta_2}}\frac{\partial}{\partial y}p_n(x,y)\Big)^2dxdy,\quad n=1,\cdots,12, \tag{2.39}$$

where $\eta=(\eta_1,\eta_2)$ and $|\eta|=\eta_1+\eta_2$.

4. Then we compute the nonlinear weights (2.15) based on the linear weights and smoothness indicators [22]. The final approximations are given by:

$$u_{G_\ell,G_{\ell\ell}}\approx\sum_{n=1}^{12}\omega_n^x(x_{G_\ell},y_{G_{\ell\ell}})\frac{\partial}{\partial x}p_n(x_{G_\ell},y_{G_{\ell\ell}}),\quad \ell,\ell\ell=1,2,3,4, \tag{2.40}$$

and

$$v_{G_\ell,G_{\ell\ell}} \approx \sum_{n=1}^{12} \omega_n^y(x_{G_\ell},y_{G_{\ell\ell}}) \frac{\partial}{\partial y} p_n(x_{G_\ell},y_{G_{\ell\ell}}), \quad \ell,\ell\ell=1,2,3,4. \tag{2.41}$$

3 Numerical tests

In this section, we set CFL number to be 0.6 and present the results of numerical tests of the new HWENO schemes specified in the previous section both in one and two dimensions on structured meshes.

Example 3.1. We solve the following nonlinear scalar one dimensional Burgers' equation:

$$\phi_t + \frac{(\phi_x+1)^2}{2} = 0, \quad -1 < x < 1, \tag{3.1}$$

with the initial condition $\phi(x,0) = -\cos(\pi x)$ and periodic boundary condition. When $t = 0.5/\pi^2$ the solution is still smooth. The errors and numerical orders of accuracy are shown in Table 1. We can see the scheme achieves its designed order of accuracy in one dimension.

Example 3.2. We solve the following nonlinear scalar one dimensional Hamilton-Jacobi equation:

$$\phi_t - \cos(\phi_x+1) = 0, \quad -1 < x < 1, \tag{3.2}$$

with the initial condition $\phi(x,0) = -\cos(\pi x)$ and periodic boundary condition. We compute the result up to $t = 0.5/\pi^2$. The errors and numerical orders of accuracy are shown in Table 2. Again, we can see the scheme achieves its designed order of accuracy in one dimension on structured meshes.

Example 3.3. We solve the following nonlinear scalar two dimensional Burgers' equation:

$$\phi_t + \frac{(\phi_x+\phi_y+1)^2}{2} = 0, \quad -2 \le x,y < 2, \tag{3.3}$$

with the initial condition $\phi(x,y,0) = -\cos(\pi(x+y)/2)$ and periodic boundary conditions. We compute the result to $t=0.5/\pi^2$ and the solution is still smooth at that time. The errors and numerical orders of accuracy by the HWENO scheme are shown in Table 3.

Example 3.4. We solve the following nonlinear scalar two dimensional Hamilton-Jacobi equation:

$$\phi_t - \cos(\phi_x+\phi_y+1) = 0, \quad -2 \le x,y < 2, \tag{3.4}$$

with the initial condition $\phi(x,y,0) = -\cos(\pi(x+y)/2)$ and periodic boundary conditions. We also compute the result until $t = 0.5/\pi^2$. The errors and numerical orders of accuracy by the HWENO scheme are shown in Table 4.

Table 1: $\phi_t+(\phi_x+1)^2/2=0$. $\phi(x,0)=-\cos(\pi x)$. Periodic boundary conditions. $t=0.5/\pi^2$.

HWENO				
cells	L^1 error	order	L^∞ error	order
10	9.92E-5		3.66E-4	
20	4.82E-6	4.36	2.72E-5	3.75
40	1.61E-7	4.90	1.15E-6	4.55
80	3.23E-9	5.64	2.82E-8	5.36
160	4.63E-11	6.12	4.83E-10	5.87
320	9.83E-13	5.56	6.77E-12	6.16

Table 2: $\phi_t-\cos(\phi_x+1)=0$. $\phi(x,0)=-\cos(\pi x)$. Periodic boundary conditions. $t=0.5/\pi^2$.

HWENO				
cells	L^1 error	order	L^∞ error	order
10	8.53E-5		2.10E-4	
20	5.63E-6	3.92	2.83E-5	2.90
40	3.53E-7	4.00	3.73E-6	2.93
80	1.69E-8	4.38	2.70E-7	3.79
160	4.17E-10	5.34	7.28E-9	5.21
320	8.26E-12	5.65	2.31E-10	4.97

Table 3: $\phi_t+(\phi_x+\phi_y+1)^2/2=0$. $\phi(x,y,0)=-\cos(\pi(x+y)/2)$. Periodic boundary conditions. $t=0.5/\pi^2$.

HWENO				
cells	L^1 error	order	L^∞ error	order
20×20	9.11E-5		4.70E-4	
40×40	3.52E-6	4.69	1.78E-5	4.72
80×80	8.41E-8	5.39	5.91E-7	4.91
160×160	9.24E-10	6.51	7.21E-9	6.36
320×320	2.64E-11	5.13	1.47E-10	5.61

Table 4: $\phi_t-\cos(\phi_x+\phi_y+1)=0$. $\phi(x,y,0)=-\cos(\pi(x+y)/2)$. Periodic boundary conditions. $t=0.5/\pi^2$.

HWENO				
cells	L^1 error	order	L^∞ error	order
20×20	3.85E-5		1.45E-4	
40×40	3.73E-6	3.37	3.18E-5	2.20
80×80	1.48E-7	4.65	1.82E-6	4.12
160×160	4.44E-9	5.06	5.99E-8	4.93
320×320	1.33E-10	5.06	1.42E-9	5.40

Example 3.5. We solve the linear equation:

$$\phi_t+\phi_x=0, \tag{3.5}$$

with the initial condition $\phi(x,0)=\phi_0(x-0.5)$ together with the periodic boundary condi-

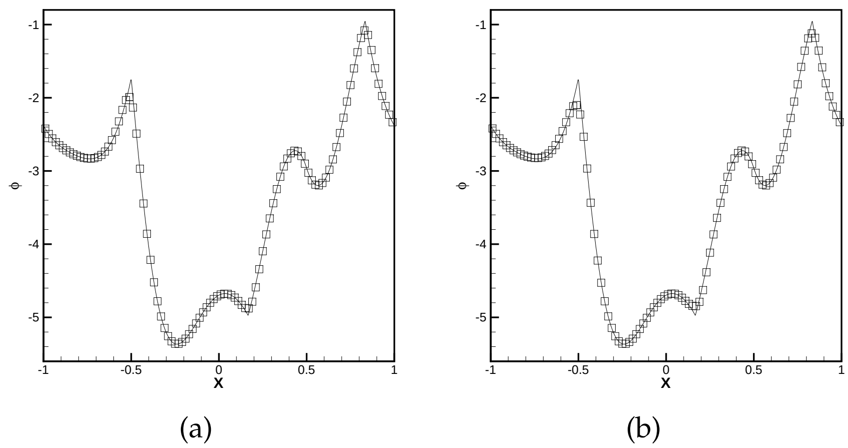

Figure 1: One dimensional linear equation. 100 cells. (a) $t=2$; (b) $t=8$. Solid line: the exact solution; square symbols: HWENO scheme.

tions, where:

$$\phi_0(x) = -\left(\frac{\sqrt{3}}{2}+\frac{9}{2}+\frac{2\pi}{3}\right)(x+1)+\begin{cases} 2\cos\left(\dfrac{3\pi x^2}{2}\right)-\sqrt{3}, & -1\leq x<-\dfrac{1}{3}, \\ \dfrac{3}{2}+3\cos(2\pi x), & -\dfrac{1}{3}\leq x<0, \\ \dfrac{15}{2}-3\cos(2\pi x), & 0\leq x<\dfrac{1}{3}, \\ \dfrac{28+4\pi+\cos(3\pi x)}{3}+6\pi x(x-1), & \dfrac{1}{3}\leq x<1. \end{cases} \tag{3.6}$$

We plot the results with 100 cells at $t=2$ and $t=8$ in Fig. 1. We can observe that the results by the HWENO scheme have good resolution for the corner singularity.

Example 3.6. We solve the one dimensional nonlinear Burgers' equation:

$$\phi_t + \frac{(\phi_x+1)^2}{2} = 0, \tag{3.7}$$

with the initial condition $\phi(x,0) = -\cos(\pi x)$ and the periodic boundary conditions. We plot the results at $t=3.5/\pi^2$ when discontinuous derivative appears. The solutions of the HWENO scheme are given in Fig. 2. We can see the scheme gives good results for this problem.

Example 3.7. We solve the nonlinear equation with a non-convex flux:

$$\phi_t - cos(\phi_x+1) = 0, \tag{3.8}$$

with the initial data $\phi(x,0) = -\cos(\pi x)$ and the periodic boundary conditions. Then we plot the results at $t=1.5/\pi^2$ in Fig. 3 when the discontinuous derivative appears in the solution. We can see that the HWENO scheme gives good results for this problem.

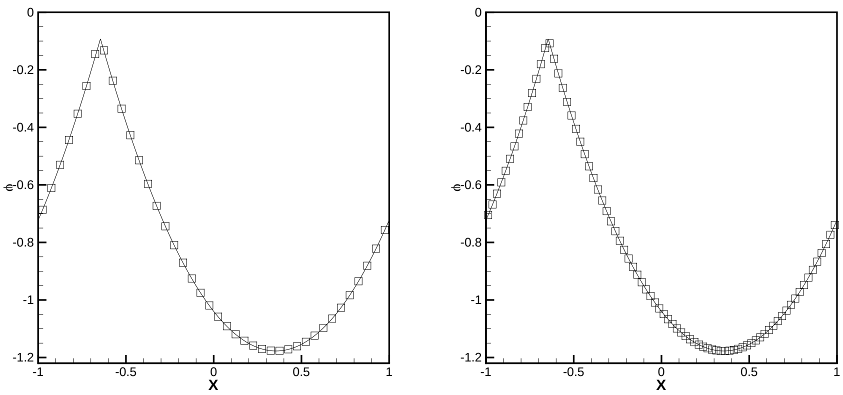

(a) (b)

Figure 2: One dimensional Burgers' equation. (a) 40 cells; (b) 80 cells. $t=3.5/\pi^2$. Solid line: the exact solution; square symbols: HWENO scheme.

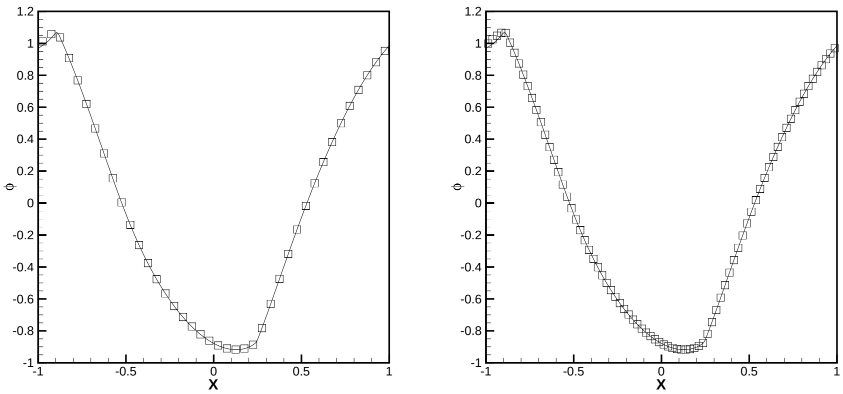

(a) (b)

Figure 3: Problem with the non-convex flux $H(\phi_x)=-\cos(\phi_x+1)$. (a) 40 cells; (b) 80 cells. $t=3.5/\pi^2$. Solid line: the exact solution; square symbols: HWENO scheme.

Example 3.8. We solve the one-dimensional Riemann problem with a non-convex flux:

$$\begin{cases} \phi_t+\dfrac{1}{4}(\phi_x^2-1)(\phi_x^2-4)=0, & -1<x<1, \\ \phi(x,0)=-2|x|. \end{cases} \tag{3.9}$$

This is a demanding test case, for many schemes have poor resolutions or could even converge to a non-viscosity solution for this case. We plot the results at $t=1$ by the scheme with 40, 80, 160, 320 and 640 cells to verify the numerical solutions' convergent property in Fig. 4. We can see that such scheme gives good results for this problem.

Example 3.9. We solve the same two dimensional nonlinear Burgers' equation (3.3) as in Example 3.3 with the same initial condition $\phi(x,y,0)=-\cos(\pi(x+y)/2)$, except that we

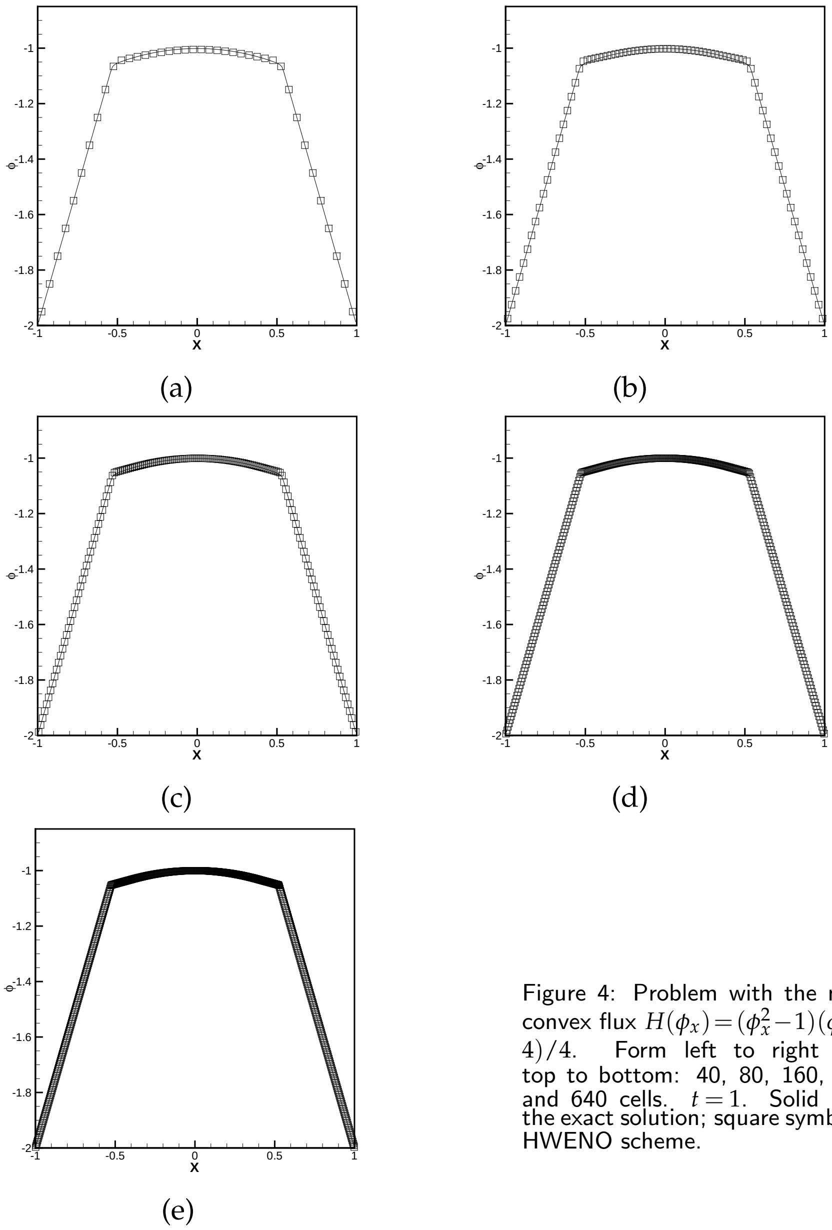

Figure 4: Problem with the non-convex flux $H(\phi_x)=(\phi_x^2-1)(\phi_x^2-4)/4$. Form left to right and top to bottom: 40, 80, 160, 320 and 640 cells. $t=1$. Solid line: the exact solution; square symbols: HWENO scheme.

now plot the results at $t=1.5/\pi^2$ in Fig. 5 when the discontinuous derivative has already appeared in the solution. We observe good resolutions for this example.

Example 3.10. The two dimensional Riemann problem with a non-convex flux:

$$\begin{cases} \phi_t+\sin(\phi_x+\phi_y)=0, \qquad -1\le x,y<1, \\ \phi(x,y,0)=\pi(|y|-|x|). \end{cases} \tag{3.10}$$

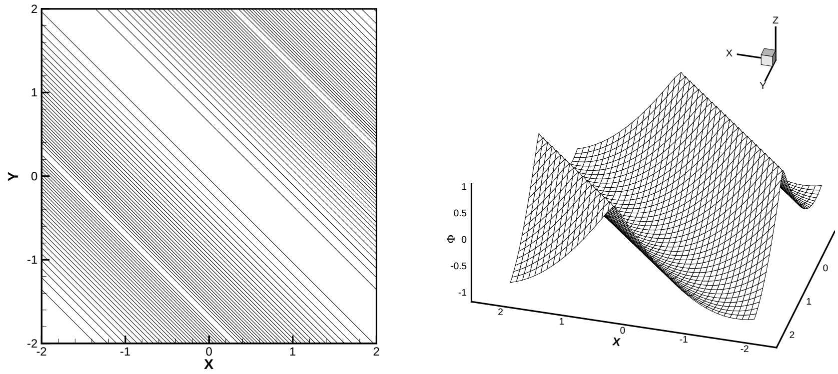

(a) (b)

Figure 5: Two dimensional Burgers' equation. 40×40 cells. $t=1.5/\pi^2$. HWENO scheme. (a) Contours of the solution; (b) the surface of the solution.

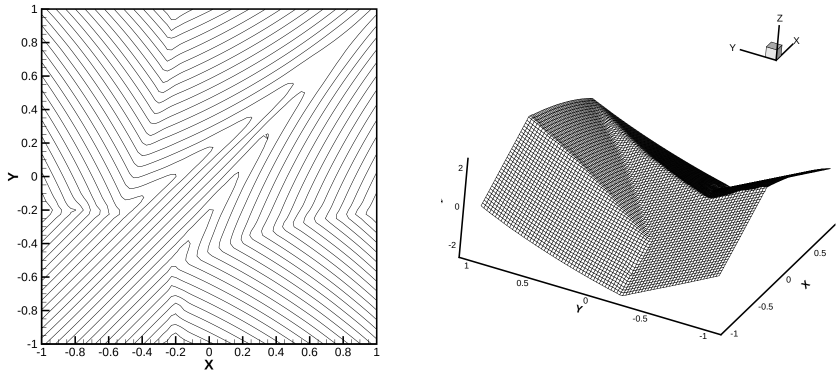

(a) (b)

Figure 6: Two dimensional Riemann problem with a non-convex flux $H(\phi_x,\phi_y)=\sin(\phi_x+\phi_y)$. 80×80 cells. $t=1$. HWENO scheme. (a) Contours of the solution; (b) the surface of the solution.

The solution of the HWENO scheme is plotted at $t=1$ in Fig. 6. We can also observe good resolutions for this numerical simulation.

Example 3.11. A problem from optimal control:

$$\begin{cases} \phi_t+\sin(y)\phi_x+(\sin(x)+sign(\phi_y))\phi_y-\dfrac{1}{2}\sin(y)^2-(1-\cos(x))=0, & \pi\le x,y<\pi, \\ \phi(x,y,0)=0, \end{cases} \tag{3.11}$$

with periodic conditions, see [15]. The solution of the HWENO scheme is plotted at $t=1$ and the optimal control $\omega=\text{sign}(\phi_y)$ is shown in Fig. 7.

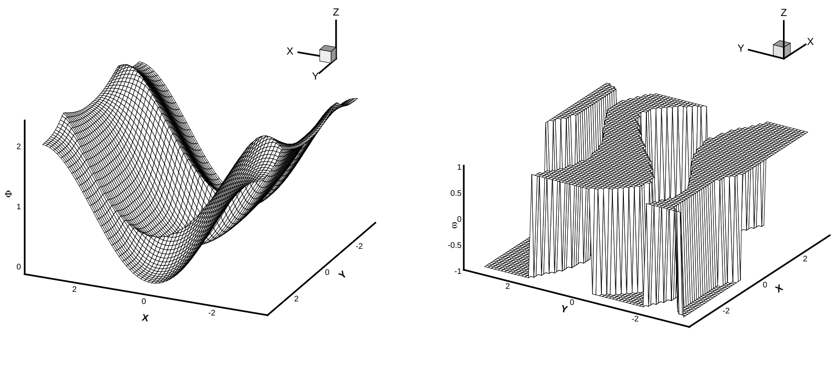

(a) (b)

Figure 7: The optimal control problem. 60×60 cells. $t=1$. HWENO scheme. (a) The surface of the solution; (b) the optimal control $\omega=\text{sign}(\phi_y)$.

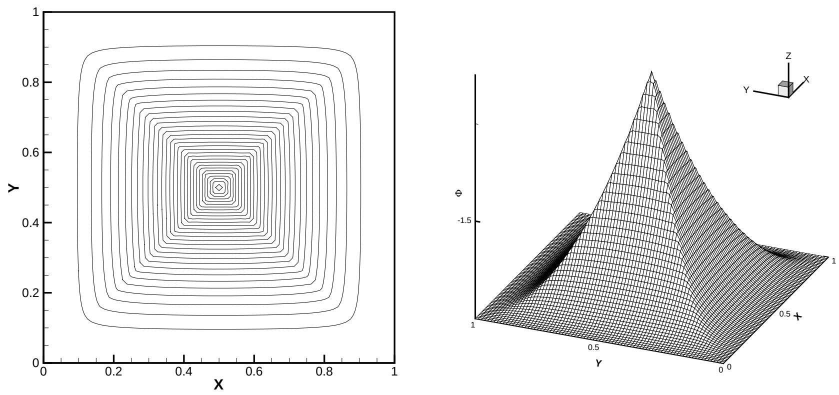

(a) (b)

Figure 8: Eikonal equation with a non-convex Hamiltonian. 80×80 cells. $t=0.6$. HWENO scheme. (a) Contours of the solution; (b) the surface of the solution.

Example 3.12. A two dimensional Eikonal equation with a non-convex Hamiltonian, which arises in geometric optics [9], is given by:

$$\begin{cases} \phi_t+\sqrt{\phi_x^2+\phi_y^2+1}=0, & 0\le x,y<1, \\ \phi(x,y,0)=\dfrac{1}{4}(\cos(2\pi x)-1)(\cos(2\pi y)-1)-1. \end{cases} \tag{3.12}$$

The solutions of the HWENO scheme are plotted at $t=0.6$ in Fig. 8. Good resolutions are observed with the proposed scheme.

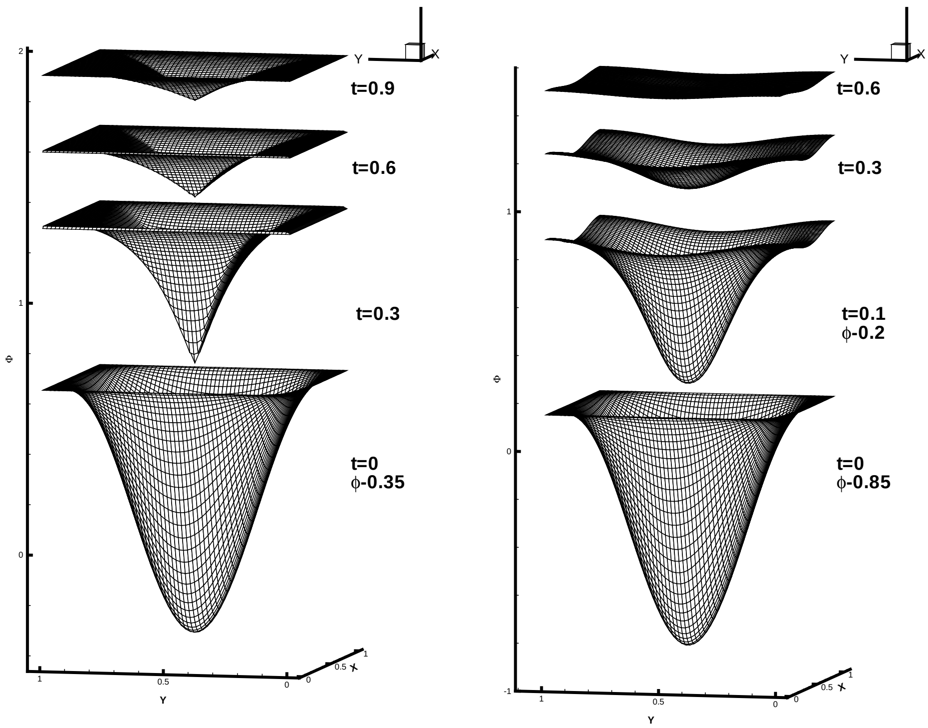

(a) (b)

Figure 9: Propagating surface. 60×60 cells. (a) $\varepsilon=0$; (b) $\varepsilon=0.1$. HWENO scheme.

Example 3.13. The problem of a propagating surface [14]:

$$\begin{cases} \phi_t-(1-\varepsilon K)\sqrt{\phi_x^2+\phi_y^2+1}=0, & 0\le x,y<1, \\ \phi(x,y,0)=1-\dfrac{1}{4}(\cos(2\pi x)-1)(\cos(2\pi y)-1), \end{cases} \tag{3.13}$$

where K is the mean curvature defined by:

$$K=-\frac{\phi_{xx}(1+\phi_y)^2-2\phi_{xy}\phi_x\phi_y+\phi_{yy}(1+\phi_x^2)}{(1+\phi_x^2+\phi_y^2)^{3/2}}, \tag{3.14}$$

and ε is a small constant. A periodic boundary conditions are used. The approximation of K is constructed by the methods similar to the first derivative terms and three different second order derivatives of associated Hermite reconstruction polynomials are needed. The results of $\varepsilon=0$ (pure convection) and $\varepsilon=0.1$ by the HWENO scheme are presented in Fig. 9. The surfaces at $t=0$ for $\varepsilon=0$ and for $\varepsilon=0.1$, and at $t=0.1$ for $\varepsilon=0.1$, are shifted downward in order to show the detail of the solution at later time.

4 Concluding remarks

In this paper, we have constructed a new class of finite volume HWENO schemes for solving the Hamilton-Jacobi equations in one and two dimensions. The main advantages of such methodologies are their compactness in spacial field, only one set of small stencils is needed on constructing different types of polynomials and are purely on the finite volume framework (not like the finite difference framework specified in [7, 16] or the nodal and cell average mixed model specified in [17, 20]). The constructions of such new HWENO schemes are based on Hermite WENO interpolation in spatial field and then Runge-Kutta discretization is used for the ODEs. In the new HWENO schemes, both the cell averaged solution and its first one (in 1D) or two (in 2D) cell averaged derivatives are evolved via time marching and used in the reconstructions and are more compact than the original HWENO schemes [17, 20]. These schemes have high order accuracy for the smooth regions, can obtain high resolutions for the singularities of the derivatives and can converge to the physical viscosity solutions compactly and robustly. Extensive numerical experiments are performed to illustrate the capability of these HWENO schemes.

Acknowledgments

The research was supported by NSFC grants 10931004, 11372005, 11002071 and 91230110.

References

[1] R. Abgrall and T. Sonar, On the use of Muehlbach expansions in the recovery step of ENO methods, Numer. Math., 76 (1997), 1–25.

[2] S. Augoula and R. Abgrall, High order numerical discretization for Hamilton-Jacobi equations on triangular meshes, J. Sci. Comput., 15 (2000), 198–229.

[3] T. J. Barth and J. A. Sethian, Numerical schemes for the Hamilton-Jacobi and level set equations on triangulated domains, J. Comput. Phys., 145 (1998), 1–40.

[4] C. K. Chan, K. S. Lau and B. L. Zhang, Simulation of a premixed turbulent Name with the discrete vortex method, Int. J. Numer. Meth. Eng., 48 (2000), 613–627.

[5] Y. D. Cheng and C.-W. Shu, A discontinuous Galerkin finite element method for directly solving the Hamilton-Jacobi equations, J. Comput. Phys., 223 (2007), 398–415.

[6] C. Hu and C.-W. Shu, A discontinuous Galerkin finite element method for Hamilton-Jacobi equations, SIAM J. Sci. Comput., 21 (1999), 666–690.

[7] G. S. Jiang and D. Peng, Weighted ENO schemes for Hamilton-Jacobi equations, SIAM J. Sci. Comput., 21 (2000), 2126–2143.

[8] G. S. Jiang and C.-W. Shu, Efficient implementation of weighted ENO schemes, J. Comput. Phys., 126 (1996), 202–228.

[9] S. Jin and Z. Xin, Numerical passage from systems of conservation laws to Hamilton-Jacobi equations, and relaxation schemes, SIAM J. Numer. Anal., 35 (1998), 2163–2186.

[10] F. Lafon and S. Osher, High order two dimensional nonoscillatory methods for solving Hamilton-Jacobi scalar equations, J. Comput. Phys., 123 (1996), 235–253.

[11] O. Lepsky, C. Hu and C.-W. Shu, Analysis of the discontinuous Galerkin method for Hamilton-Jacobi equations, Appl. Numer. Math., 33 (2000), 423–434.

[12] X. G. Li and C. K. Chan, High-order schemes for Hamilton-Jacobi equations on triangular meshes, J. Comput. Appl. Math., 167 (2004), 227–241.

[13] P. L. Lions, Generalized Solutions of Hamilton-Jacobi Equations, Pitman, London, 1982.

[14] S. Osher and J. Sethian, Fronts propagating with curvature dependent speed: algorithms based on Hamilton-Jacobi formulations, J. Comput. Phys., 79 (1988), 12–49.

[15] S. Osher and C.-W. Shu, High-order essentially nonoscillatory schemes for Hamilton-Jacobi equations, SIAM J. Numer. Anal., 28 (1991), 907–922.

[16] J. Qiu, WENO schemes with Lax-Wendroff type time discretizations for Hamilton-Jacobi equations, J. Comput. Appl. Math., 200 (2007), 591–605.

[17] J. Qiu, Hermite WENO schemes with Lax-Wendroff type time discretizations for Hamilton-Jacobi equations, J. Comput. Math., 25 (2007), 131–144.

[18] J. Qiu and C.-W. Shu, Hermite WENO schemes and their application as limiters for Runge-Kutta discontinuous Galerkin method: one dimensional case, J. Comput. Phys., 193 (2004), 115–135.

[19] J. Qiu and C.-W. Shu, Hermite WENO schemes and their application as limiters for Runge-Kutta discontinuous Galerkin method II: two-dimensional case, Comput. Fluids, 34 (2005), 642–663.

[20] J. Qiu and C.-W. Shu, Hermite WENO schemes for Hamilton-Jacobi equations, J. Comput. Phys., 204 (2005), 82–99.

[21] J. A. Sethian, Level Set Methods and Fast Marching Methods, Evolving Interface, Computational Geometry, Fluid Mechanics, Computer Vision, and Materials Science, Cambridge University Press, Cambridge, 1999.

[22] C.-W. Shu, Essentially non-oscillatory and weighted essentially non-oscillatory schemes for hyperbolic conservation laws, in Advanced Numerical Approximation of Nonlinear Hyperbolic Equations. edited by A. Quarteroni, Editor, Lecture Notes in Mathematics, CIME subseries (Springer-Verlag, Berlin/New York); ICASE Report 97–65, 1997.

[23] C.-W. Shu and S. Osher, Efficient implementation of essentially non-oscillatory shock capturing schemes, J. Comput. Phys., 77 (1988), 439–471.

[24] J. Yan and S. Osher, A local discontinuous Galerkin method for directly solving Hamilton-Jacobi equations, J. Comput. Phys., 230 (2011), 232–244.

[25] Y. T. Zhang and C.-W. Shu, High-order WENO schemes for Hamilton-Jacobi equations on triangular meshes, SIAM J. Sci. Comput., 24 (2003), 1005–1030.

[26] J. Zhu and J. Qiu, A class of the fourth order finite volume Hermite weighted essentially non-oscillatory schemes, Science in China, Series A-Mathematics, 51 (2008), 1549–1560.

[27] J. Zhu and J. Qiu, Hermite WENO schemes and their application as limiters for Runge-Kutta discontinuous Galerkin method III: unstructured meshes, J. Sci. Comput., 39 (2009), 293–321.